Report no. changed (Mar 2006): SM-320-UU

SACLANTCEN MEMORANDUM
serial no.: SM-320

SACLANT UNDERSEA
RESEARCH CENTRE
MEMORANDUM

MODELLING SCATTERING FROM PARTIALLY BURIED CYLINDERS

J.A. Fawcett

December 1996

Report no. changed (Mar 2006): SM-320-UU

SACLANT Undersea Research Centre
Viale San Bartolomeo 400
19138 San Bartolomeo (SP), Italy

tel: +39-187-540.111
fax: +39-187-524.600

e-mail: library@saclantc.nato.int

NORTH ATLANTIC TREATY ORGANIZATION

SACLANTCEN SM-320

Modelling scattering from partially buried cylinders

John. A Fawcett

The content of this document pertains to work performed under Project 033-3 of the SACLANTCEN Programme of Work. The document has been approved for release by The Director, SACLANTCEN.

Jan L. Spoelstra
Director

intentionally blank page

Modelling scattering from partially buried cylinders

John A. Fawcett

Executive Summary:

A better understanding of how energy is scattered in the ocean will lead to a significant improvement in our ability to detect and classify scattering objects such as mines. In particular, in this memorandum, we consider the case of a cylinder partially buried in a sediment. The scattering characteristics of the cylinder in this case are significantly different than if the cylinder was totally surrounded by, for example, water and will, in fact, depend upon the degree of burial.

This memorandum describes two approaches to computing the scattering from partially buried cylinders. The first approach allows one to compute the scattered field in an efficient manner for a cylinder which is buried 50% in a lower sediment having a different density than water but the same sound speed. This is a very particular problem, but the solution can be computed in an efficient and accurate manner and hence can be used as a benchmark solution for more general computational methods. The second approach which is described can be used to compute the scattering from partially buried cylinders in more realistic sediments. This method is used to compute the amplitude of the energy backscattered from a cylinder as a function of frequency and the cylinder's degree of burial in the sediment.

intentionally blank page

Modeling scattering from partially buried cylinders

John A. Fawcett

Abstract: 1. A boundary integral equation method is presented for the computation of the acoustic field scattered from a cylindrical object which is totally within the water column, totally buried in sediment, or partially buried. The unknown field quantities within the cylindrical object (which may have internal cylindrical layering) are represented by a Fourier/Bessel series with unknown coefficients. The pressure field and its radial derivative on the exterior of the cylinder are related to this series and a system of equations for the unknown coefficients derived. This method is used to compute the spectral curves for the backscattered field as a function of cylinder burial. Some two-dimensional full-field computations for scattering from cylindrical objects are also presented.

2. Various methods have been proposed for the solution of waveguide scattering problems(1-3). The last two references however are not applicable in the case of a scattering object embedded in an interface between two media. A semi-analytical solution is given to the problem of a cylinder embedded between two half-spaces with only a discontinuity in density (although the sound speed can be different within the cylinder). Although this is a particular subset of the general scattering problem, this method could provide useful benchmarks for more general numerical codes.

Keywords: Sea surface scattering - Bottom scattering - Mine detection

Contents

Acoustic scattering from cylindrical objects embedded between two half-spaces

John A. Fawcett
SACLANT Undersea Research Centre, Viale San Bartolomeo 400, 19138 San Bartolomeo, La Spezia, Italy

(Received 13 February 1996; accepted for publication 13 June 1996)

In this paper a boundary integral equation method is presented for the computation of the acoustic field scattered from a cylindrical object which is totally within the water column, totally buried in sediment, or partially buried. The unknown field quantities within the cylindrical object (which may have internal cylindrical layering) are represented by a Fourier/Bessel series with unknown coefficients. The pressure field and its radial derivative on the exterior of the cylinder are related to this series and a system of equations for the unknown coefficients derived. This method is used to compute the spectral curves for the backscattered field as a function of cylinder burial. Some two-dimensional full-field computations for scattering from cylindrical objects are also presented.

PACS numbers: 43.30.Gv, 43.20.Fn [MBP]

INTRODUCTION

Boundary integral equation methods[1] (BIEM), T-matrix methods (see, for example, Ref. 2) and wave field superposition methods[3] have been described for the solution of scattering problems in a waveguide. Generally, T-matrix methods have not been applied to the case of a partially buried object; however, some recent T-matrix work does consider this problem.[4] It may also be possible to use the ideas of wave field superposition for the case of the partially buried scatterer; we have not investigated this concept.

The BIEM of Ref. 1 can be used to solve many types of elastic object/waveguide scattering problems. The method of this paper has advantages for the computation of scattering in cylindrical object/two half-space problems. The method combines the form of the interior cylinder solution with the exterior two half-space Green's function. Because of the method's formulation, it is straightforward to include any cylindrical layering in the problem without a significant increase in computational effort. The singular portions of the exterior Green's function are isolated and treated with care; because these singularities are subtracted from the wave-number integrals, the remaining wave-number integrands are more rapidly convergent as a function of the horizontal wave number.

In the numerical examples, we use our method to compute the spectral characteristics of the pressure field backscattered from a cylinder for varying amounts of burial in the sediment. We also compute and display the two-dimensional pressure field for two examples of a partially buried cylinder; a solid cylinder example and a shelled-cylinder example.

I. THEORY

Consider a half-space with the upper medium having sound speed c_1 and density ρ_1 and the lower medium, sound speed c_2 and density ρ_2. A cylinder with sound speed c_c, density ρ_c and radius a is embedded fractionally between the two medium (see Fig. 1). The x-z coordinates are defined by $x=r\sin\theta$ and $z=r\cos\theta$, where θ is indicated in Fig. 1. We are considering two-dimensional scattering in this paper, or equivalently, the cylinder, the waveguide, and the source can be thought of as being infinite in extent (in one direction) in a three-dimensional waveguide. The method described will also handle the case where the object is entirely within one of the two media. In this paper we consider an acoustic medium and cylinder, but many of the same concepts, described below, could also be applied to an elastic problem.

From Gauss's divergence theorem[5] we can write

$$p(r,\theta)=p^{\text{inc}}+a\int_0^{2\pi}G_{r'}(r,\theta;r'=a,\theta')p(a,\theta')d\theta' - a\int_0^{2\pi}G(r,\theta;r'=a,\theta')p_{r'}(a,\theta')d\theta'. \quad (1)$$

Because of the interface conditions satisfied by $G(r,\theta;r',\theta')$ and $p(r,\theta)$ at the interface $z=-L$, it can be shown that Eq. (1) is valid for the cylinder above, below, or embedded in the interface. In Eq. (1) $p(a,\theta')$ and $p_{r'}(a,\theta')$ refer to values of the pressure field and its radial derivative on the exterior surface of the cylinder. Below, we derive a series solution expression for the pressure field and its radial derivative in the interior of the cylinder and then relate these to the exterior values.

A. Representation of interior solution

In this paper the cylindrical object may have internal layering. We will consider two cases in detail here; a homogeneous cylinder and a cylinder with a shell. In the first case, the pressure field within the cylinder p^{in} has the representation

$$p^{in}(r,\theta)=\sum_{n=-N}^{N}a_nJ_n(kr)e^{in\theta} \quad (2a)$$

and

$$p_r^{in}(r,\theta)=\sum_{n=-N}^{N}a_n\frac{dJ_n(kr)}{dr}e^{in\theta}. \quad (2b)$$

 0001-4966/96/100(5)/3053/8/$10.00

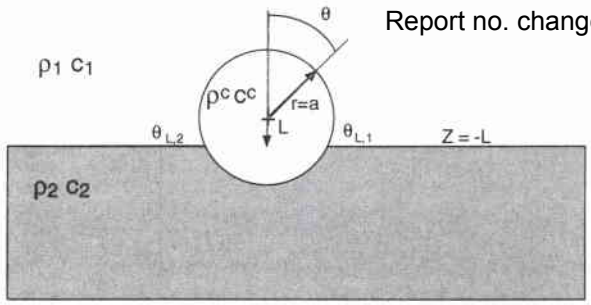

FIG. 1. Schematic diagram of cylinder embedded between two half-spaces.

At the surface of the cylinder $r=a$ we can absorb the Bessel functions into the coefficients and write

$$p^{in}(a,\theta)=\sum_{n=-N}^{N}\hat{a}_n e^{in\theta} \tag{3a}$$

and

$$p_r^{in}(a,\theta)=\sum_{n=-N}^{N}\hat{a}_n\gamma_n e^{in\theta}. \tag{3b}$$

For a homogeneous cylinder

$$\gamma_n\equiv\frac{J_n'(ka)}{J_n(ka)}, \tag{3c}$$

where a prime denotes differentiation with respect to r. In the case that $J_n(ka)=0$, the representations of Eqs. (2a) and (2b) should be used.

The case of a cylinder with a shell can also be handled straightforwardly. Suppose that the cylinder has an inner layer at $r=b$. We will suppose that the wave number in this inner region is $k_1^c=\omega/c_1$ and the density is ρ_1^c. Within the outer layer of the cylinder there are the values $k_2^c=\omega/c_2$ and ρ_2^c (see Fig. 2). Within the inner region the pressure field has the form

$$p^{in}(r,\theta)=\sum_{n=-N}^{N}c_n J_n(k_1^c r)e^{in\theta}. \tag{4a}$$

In the outer shell the solution has the form

$$p^{in}(r,\theta)=\sum_{n=-N}^{N}[a_n J_n(k_2^c r)+b_n H_n(k_2^c r)]e^{in\theta}. \tag{4b}$$

Satisfying the continuity equations at $r=b$ leads to the relation $b_n=d_2/d_1 a_n$, where

$$d_2=\frac{J_n(k_1^c b)J_n'(k_2^c b)}{\rho_2^c}-\frac{J_n(k_2^c b)J_n'(k_1^c b)}{\rho_1^c} \tag{5a}$$

and

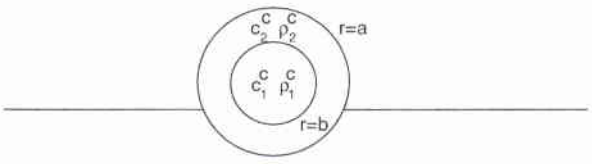

FIG. 2. Schematic diagram of layered cylinder.

$$d_1=\frac{J_n(k_1^c b)H_n'(k_2^c b)}{\rho_1^c}-\frac{J_n(k_1^c b)H_n'(k_2^c b)}{\rho_2^c}. \tag{5b}$$

This means that as before we can use Eqs. (3a) and (3b) at $r=a$, where now

$$\gamma_n\equiv\frac{J_n'+d_2/d_1 H_n'}{J_n+d_2/d_1 H_n}\,(r=a). \tag{6}$$

The chief point to note is that in both cases (and in general for layered cylinders) we can express the acoustic field quantities at the surface of the cylinder in terms of a sequence of unknown coefficients.

B. Representation of the exterior solution

The form of the acoustic field quantities derived in Sec. I A is valid inside the cylinder. However, in the integral representation of Eq. (1) we require the field on the exterior surface of the cylinder. From the boundary conditions at the surface of the cylinder, we know that the pressure field is continuous and hence we can use the representation of Eq. (3a) for this quantity. The radial derivative of the field normalized by the density is also continuous at the surface of the cylinder. Hence for the integration point in the upper medium we can use for the exterior field quantities, $p_r(\theta')=(\rho_1/\rho_c)p_r^{in}(\theta')$ and in the lower medium $p_r(\theta')=(\rho_2/\rho_c)p_r^{in}(\theta')$, where ρ_c denotes the density of the outermost layer of the cylinder.

Substituting these expressions into Eq. (1) the following relation is found:

$$p(r,\theta)=p^{\text{inc}}+a\int_0^{2\pi}G_{r'}(r,\theta;a,\theta')\sum_{n=-N}^{N}\hat{a}_n e^{in\theta}\,d\theta' - a\int_0^{2\pi}G(r,\theta;a,\theta')\alpha(\theta')\sum_{n=-N}^{N}\hat{a}_n\gamma_n e^{in\theta}\,d\theta', \tag{7}$$

where

$$\alpha(\theta')=\begin{cases}\rho_1/\rho_c, & 0\leq\theta'\leq\theta_{L,1},\quad \theta_{L,2}\leq\theta'\leq 2\pi\\ \rho_2/\rho_c, & \theta_{L,1}\leq\theta'\leq\theta_{L,2},\end{cases} \tag{8}$$

and γ_n is defined in Eq. (3c) or (6). The angle θ' is defined with respect to the center of the cylinder and the angles $\theta_{L,1}$ and $\theta_{L,2}$ are those of Fig. 1.

We now consider the limit of Eq. (7) as the observation range approaches the cylinder $r\to a$; we also multiply both sides of Eq. (7) by $e^{-im\theta}$ and integrate from 0 to 2π to obtain

$$2\pi\hat{a}_m=i_m+A_{mn}\hat{a}_n-B_{mn}\hat{a}_n, \tag{9a}$$

where

$$A_{mn}\equiv a\int_0^{2\pi}\int_0^{2\pi}G_{r'}(a+\epsilon,\theta;a,\theta')e^{-im\theta}e^{in\theta'}\,d\theta\,d\theta', \tag{9b}$$

$$B_{mn}\equiv a\int_0^{2\pi}\int_0^{2\pi}G(a+\epsilon,\theta;a,\theta')\alpha(\theta')\times e^{-im\theta}\,e^{in\theta'}\,d\theta\,d\theta', \tag{9c}$$

and

$$i_m \equiv \int_0^{2\pi} p^{\mathrm{inc}}(\theta) e^{-im\theta}\, d\theta. \tag{9d}$$

It is important to note that we have not included in Eq. (9a) the usual factor of $\frac{1}{2}$ from the singular behavior of the integral[5] of Eq. (9b) as $r \to r'$. This is because of the manner in which we will perform this integration; in particular, we will consider an azimuthal expansion of $G_{r'}$ valid for $r > r'$ [for example, we will have radial terms of the form $H_n(kr)J_{n,r'}(kr')$ in the expansion], we perform the integrations with respect to θ and θ' with this range assumption, and then take the limit as $r \to a$. In this manner the singular limit in Eq. (9b) is properly accounted for and it is not necessary to explicitly indicate the factor of $\frac{1}{2}$ in Eq. (9a) [see, also, the discussion of Eq. (14)].

Equations (9a)–(9d) are the fundamental equations of this paper. The solution of these equations (i.e., equivalent to the inversion of the matrix $B_{mn} - A_{mn} + \delta_{mn}$, where $\delta_{m,n}$ is the Kronecker delta function) yields the interior Fourier coefficients $\{\hat{a}_n, n = -N, \ldots, N\}$, which through Eq. (7) can be used to compute the pressure field anywhere within the waveguide. From the work of Schenck[6] and others it is known that for some exterior scattering problems, BIEM implementations may break down at certain frequencies. We have not rigorously analyzed our particular class of problems but, at least for the cases that we have computed thus far, we have not encountered this problem. There is an annoyance in Eqs. (3a) and (3c) when $J_n(ka) = 0$ and $\gamma_n = \infty$, but this problem is easily avoided by redefining the coefficient $\hat{a}_n$. In the remainder of this section we discuss the computation of the integrals of Eqs. (9b)–(9d).

C. Spectral representation of the Green's function

In order to evaluate the integrals of Eq. (9), we first consider the spectral representation of the waveguide Green's function. For example, considering the source point (x', z') in the upper half-space we can write[7]

$$G(x,z;x',z') = \frac{1}{2\pi} \int_{-\infty}^{\infty} e^{-ik_x(x-x')} \left[\frac{e^{i\gamma_1|z-z'|}}{2i\gamma_1} + \frac{R(k_x)}{2i\gamma_1} e^{i\gamma_1(2L+z+z')} \right] d\zeta(k_x) \tag{10a}$$

for x, z in the upper medium and

$$G(x,z;x',z') = \frac{1}{2\pi} \int_{-\infty}^{\infty} e^{-ik_x(x-x')} \frac{T(k_x)}{2i\gamma_1} \times e^{i(\gamma_1 z' - \gamma_2 z)} e^{i(\gamma_1 - \gamma_2)L}\, d\zeta(k_x) \tag{10b}$$

for x, z in the lower medium. The functions $R(k_x)$ and $T(k_x)$ are the plane-wave reflection coefficients at the interface and are given by

$$R(k_x) = \frac{\rho_2\gamma_1 - \rho_1\gamma_2}{\rho_2\gamma_1 + \rho_1\gamma_2} \tag{11a}$$

and

$$T(k_x) = \frac{2\rho_2\gamma_1}{\rho_2\gamma_1 + \rho_1\gamma_2}, \tag{11b}$$

where

$$\gamma_i \equiv \sqrt{\omega^2/c_i^2 - k_x^2}. \tag{11c}$$

Similar expressions can be written for x', z' in the lower medium. It is advantageous to perform the integrations of Eqs. (10a) and (10b) slightly off the real axis to avoid the singular behavior of the integrand for $\gamma_i = 0$; we denote a general integration contour in the complex plane as $\zeta(k_x)$.

We now note that for $k_x \to \infty$, $\gamma_1 = \gamma_2 = ik_x$. Hence $R(k_x) \to (\rho_2 - \rho_1)/(\rho_2 + \rho_1) \equiv R^{\infty}$ and $T(k_x) \to [2\rho_2/(\rho_2 + \rho_1)] \equiv T^{\infty}$. Using these asymptotic limits it is possible to rewrite Eq. (10a) and Eq. (10b) isolating the singular terms. In particular, we can write for (x,z) and (x',z') in the upper medium,

$$G(x,z;x',z') = \frac{i}{4} H_0^1(k_1 r_D) + \frac{i}{4} R^{\infty} H_0^1(k_1 r_R) + \frac{1}{2\pi} \int_{-\infty}^{\infty} e^{-ik_x(x-x')} \frac{(R(k_x) - R^{\infty})}{2i\gamma_1} \times e^{i\gamma_1(2L+z+z')}\, d\zeta(k_x). \tag{12a}$$

In Eq. (12a)

$$r_D \equiv \sqrt{(x-x')^2 + (z-z')^2},$$

$$r_R \equiv \sqrt{(x-x')^2 + (z+z'+2L)^2}.$$

Similarly we can write for Eq. (10b),

$$G(x,z;x',z') = \frac{i}{4} T^{\infty} H_0^1(kr_D) + \frac{1}{2\pi} \int_{-\infty}^{\infty} e^{-ik_x(x-x')} \times \left\{ \frac{T(k_x) e^{i\phi_1(k_x)} - T^{\infty} e^{i\phi_2(k_x)}}{2i\gamma_1} \right\} d\zeta(k_x), \tag{12b}$$

where

$$\phi_1(k_x) = \gamma_1 z' - \gamma_2 z + (\gamma_1 - \gamma_2)L \tag{12c}$$

and

$$\phi_2(k_x) = \gamma_1(z' - z). \tag{12d}$$

There are similar expressions for the source in the lower medium. If the cylinder is totally within a single medium then only the expressions corresponding to direct and reflected energy need to be considered.

Thus we have separated the Green's function into analytical singular terms and a remainder term which has to be numerically evaluated. Because we explicitly evaluate the integrals of the integrands' asymptotic limits (these are the Hankel function terms), the remaining numerical integrals are more rapidly convergent. It is interesting to note that for a medium with only a density contrast across the interface the singular term expansion is complete; the integral remainders are zero. This is related to the fact that for the density contrast only situation it is possible to derive a modal expansion of the solution.[8]

D. Azimuthal expansion of Green's function

It can be seen from Eqs. (9) that we must project functions of the form $e^{im\theta}$ etc. onto the Green's function and its radial derivative. In order to use our expressions for the waveguide's Green's function, the integrals are broken down into four subintervals: corresponding to source (θ') points and observation (θ) points both in the upper half-space, source and observation points both in the lower half-space, the source points in the lower half-space and observation points in the upper half-space and finally, the observation points in the lower half-space and the source points in the upper half-space.

The integrals with respect to the singular terms can be done analytically. For the direct and transmitted terms we use the expansions

$$H_0^1(kr_D)=\sum_{n=-N}^{N} H_n^1(k(a+\epsilon))J_n(ka)e^{in(\theta-\theta')} \tag{13a}$$

and

$$\frac{\partial H_0^1(kr_D)}{\partial r'}=\sum_{n=-N}^{N} H_n^1(k(a+\epsilon))\frac{dJ_n(ka)}{dr'}e^{in(\theta-\theta')}. \tag{13b}$$

These expansions are valid for all θ and θ' provided that $r>r'$ and will converge approximately as $(r_</r_>)^n$ for large n (see for example the large n asymptotics of J_n and Y_n as given in Ref. 9). Thus for $r>r'=a$ we can use the expansions of Eq. (13) in the integrals of Eq. (9) for integrating this portion of the Green's function. It is not difficult to show then that for $r>r'$, integrals of the form

$$\int_\theta\int_{\theta'}\sum_{l=-N}^{N} H_l(kr)\frac{dJ_l(ka)}{dr'}e^{il\theta}e^{-il\theta'}e^{-im\theta}e^{in\theta'}\,d\theta\,d\theta' \tag{14}$$

converge as a function of N, and that the limit as $r\to a$ is obtained by simply replacing r in Eq. (14) with a. Because we are evaluating Eq. (9b) in the limit as $r\to r'$ for $r>r'$ the singular nature of the Green's function is correctly accounted for and the usual limiting factor of $\frac{1}{2}$ required by many BIEM implementations[5] is not needed in front of the integral involving $G_{r'}$.

The singular term for the reflected field $R^\infty H_0^1(k_1r_R)$ (more particularly its radial derivative, $\partial H_0^1(k_1r_R)/\partial r'$), is more difficult to expand in terms of the azimuthal exponential functions of θ and θ'. It is possible to use the translation theorem[10] for Bessel/Hankel functions and express the reflected term as a double sum of azimuthal terms. However, the convergence of this series for the radial derivative is very poor for the region where z and z' are approximately equal to $-L$. For the results of this paper, we used a more brute-force approach—we evaluated numerically double integrals (for both the upper and lower half-spaces) of the form

$$\int_{\theta_1}^{\theta_2}\int_{\theta_1}^{\theta_2} H_0^1(kr_R(\theta,\theta'))e^{-im\theta}e^{in\theta'}\,d\theta\,d\theta' \tag{15a}$$

and

$$\int_{\theta_1}^{\theta_2}\int_{\theta_1}^{\theta_2}\frac{\partial H_0^1(kr_R(\theta,\theta'))}{\partial r'}e^{-im\theta}e^{in\theta'}\,d\theta\,d\theta'. \tag{15b}$$

To improve the behavior of the integrand in the case of the radial derivative, we subtract a term $t(\theta,\theta')$ containing the singular nature of the radial derivative and then add the analytic integral of this term to the result. In particular,

$$t(\theta,\theta')=\frac{-2i}{\pi}\frac{\{-[x(\theta)-x'(\theta')]\sin(\theta')+[z(\theta)+z'(\theta')+2L]\cos(\theta')\}}{\{[x(\theta)-x'(\theta')]^2+[z(\theta)+z'(\theta')+2L]^2\}}. \tag{16}$$

For the θ' integration, the denominator term in Eq. (16) is expanded about the midpoint of each θ' panel, up to including second-order terms in θ'. The resulting expression can be integrated analytically and gives rise to an expression containing an Arctan function.

This analytic integration is particularly important for θ and θ' approximately equal to $\theta_{L,1}$ or $\theta_{L,2}$ (see Fig. 1). A similar approach to integrating a waveguide Green's function was outlined in Ref. 11.

Finally, we must consider the wave-number integrals and their decomposition into the azimuthal exponential functions. First we note that for a fixed value of k_z that the integrands of Eqs. (12) are composed of a plane-wave components for both the (x,z) and (x',z') coordinates. These plane waves can be expanded analytically in the form

$$e^{-i(k_xx-\gamma_iz)}=\sum_{n=-\infty}^{\infty} i^nJ_n(kr)e^{in(\theta+\psi_i)}, \tag{17}$$

where $x=r\sin\theta$, $z=r\cos\theta$, and $\psi_i=\cos^{-1}(\gamma_i/k)$. The same type of expansion is also used for the plane wave in the x',z' coordinates. Substituting these type of expansions into the wave-number integrals the explicit dependence on r,r', θ, and θ' can be brought out of the wave-number integral and the azimuthal integrals performed analytically. However, there remains integrals to evaluate numerically. For example, for the reflection term (upper half-space) we have wave-number integrals of the form

$$\frac{1}{2\pi}\int_{-\infty}^{\infty}\frac{[R(k_x)-R^\infty]}{2i\gamma_1}e^{i\gamma_1 2L}e^{i(m-n)\psi_1(k_x)}\,d\zeta(k_x) \tag{18a}$$

to evaluate, and for the transmission integrals

$$\frac{1}{2\pi}\int_{-\infty}^{\infty}\left\{\frac{T(k_x)e^{i(\gamma_1-\gamma_2)L}e^{i[m\psi_1(k_x)+n\psi_2(k_x)]}-T^{\infty}e^{i(m+n)\psi_1(k_x)}}{2i\gamma_1}\right\}d\zeta(k_x). \tag{18b}$$

The wave-number integrals contain evanescent plane waves for $k_x \geq \omega/c_i$. The plane wave expansion of Eq. (17) is still valid; however, the convergence properties of this series become increasingly poor as $k_x \to \infty$. The phase $\psi_i = \cos^{-1}(\gamma_i/k)$ is now complex and $e^{in\psi_i}$ or $e^{-in\psi_i}$ grows approximately as $(2|k_x|)^n$ for large $|k_x|$. Thus for increasingly large values of $|k_x|$ it becomes necessary to use an increasing number of terms in Eq. (17) to ensure convergence of the series. If the cylinder is totally above or below an interface, then the exponential decay of the plane waves means that it is not necessary to include very much evanescent energy in the wave-number integrals and the expansions outlined above provide an efficient integration scheme. However, for the cylinder entering the interface it is necessary to include more of the evanescent energy and the Fourier–Bessel expansion of the integrand becomes more problematic. A brute-force but efficient alternative approach to this problem is not to use Eq. (17), but instead to numerically compute for each discrete point of the wave-number integrand, the integrals

$$\int_{\theta_1}^{\theta_2} e^{ia[k_x \sin(\theta)+\gamma_i \cos(\theta)]}e^{-im\theta}\,d\theta \tag{19a}$$

and

$$\int_{\theta_1}^{\theta_2} e^{ia[-k_x \sin(\theta')+\gamma_i \cos(\theta')]}e^{in\theta'}\,d\theta', \tag{19b}$$

where θ_1 and θ_2 denote the appropriate angular limits of integration in the upper or lower half-space. These are one-dimensional integrals; the double integrals for the term A_{mn} are simply obtained from the wave-number integrals of the product of these integrals. The discrete phase factors of the form $e^{im\theta_j'}$ $(j=1,\ldots,N_{az})$ are precomputed for the integrations in the upper and lower half-spaces—in this manner, the numerical azimuthal integrations are done very efficiently. In the evanescent regime of the wave-number spectrum this procedure proved to be as fast and more robust than having to use many terms in the Bessel function expansion in order to obtain stable numerical results.

In summary, there are four different domains for the Green's function (i) source and observation point are both in upper layer (ii) source in upper layer, observation point in lower layer, (iii) source in lower layer, observation point in upper layer and finally, (iv) source and observation points are both in the lower layer. For each of these cases we extract the singular behavior of the Green's function, these singular functions can then be expanded in terms of θ and θ' analytically. However, the expansion of the singular reflection term proves to be problematic, particularly for partially buried cylinders. We resorted to numerical integration with singularity subtraction to handle this term. There remains wave-number integrals for each of the reflection and transmission terms with better convergence properties as a function of k_x as a result of the singularity extractions. The plane-wave components in these integrands can be expanded in terms of θ and θ' and Bessel functions and the angular projections done analytically (although, the integration with respect to wave number must be done numerically). However, when the cylinder is only partially buried, it is generally necessary to include a significant amount of evanescent energy in the wave number integrals. Because of this problem, we used numerical integration in order to compute the azimuthal projections. For each value of the horizontal wave number k_x, a sequence of azimuthal integrations is performed with respect to θ and another sequence with respect to θ'; the various required two-dimensional integrals are formed from the products of the integrals from these two sequences. We attempt to make these numerical integrations as efficient as possible by precomputing and storing all the azimuthal phase factors which are used repeatedly in the computations.

II. NUMERICAL EXAMPLES

In the first example we consider a cylinder of radius 1 m with an interior sound speed $c_c = 5000$ m/s and $\rho_c = 3000$ kg/m^3. The upper half-space has a sound speed $c_1 = 1500$ m/s and $\rho_1 = 1000$ kg/m^3. The lower half-space has sound speed $c_2 = 1700$ m/s and $\rho_2 = 1500$ kg/m^3. A point source (line source, since we are considering a two-dimensional problem) is located at $x_s = -50$ m and $z_s = 25$ m, where the origin of the coordinate system is taken to be the centre of the cylinder. We compute the amplitude of the scattered field at this source point as a function of frequency. In Fig. 3, we show the resulting curve for this cylinder in free-space with the same parameters as the upper half-space (solid line) and with the parameters of the lower half-space (dashed line). As can be seen the two curves are very similar. The direct incident field is proportional to $H_0^1(kr_s)$ where r_s denotes the range of

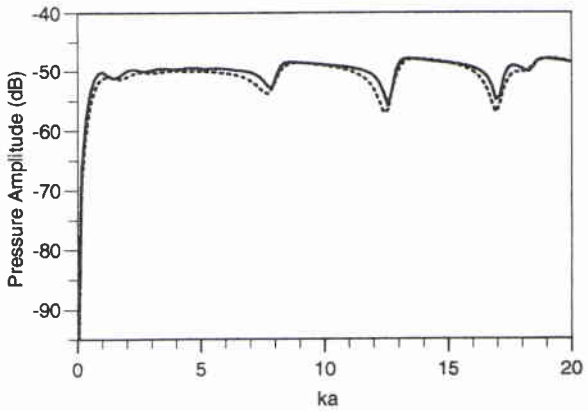

FIG. 3. Spectrum of backscattered field for 1-m-radius cylinder $c_c = 5000$ m/s, $\rho_c = 3000$ kg/m^3 ($x_s = -50$ m $z_s = 25$ m) for surrounding homogeneous space $c = 1500$ m/s (solid line), and $c = 1700$ m/s (dashed line).

the source. For large kr_s this function decays as $(kr_s)^{-1/2}$. In these curves and all other spectral curves computed in this paper, we first multiply the pressure amplitude by $\sqrt{ka}$ in order to offset this $k^{-1/2}$ dependence of the incident field. In Fig. 4(a)–(e) we show the spectral curves as computed for the cylinder centre 1.01 m above the interface (almost resting on the interface), 0.5 m above the interface (25% burial), on the interface (50% burial), 0.5 m below the interface, and 1.01 m below the interface. We used 1.01 m instead of 1.0 m for two of the curves as the form of our singularity treatment for the reflection term broke down in the case of the cylinder lying tangent to the interface—we avoided this problem by using an offset of 1.01 m instead of 1.0 m. The curves are computed for 125 equispaced frequencies—in order to produce smooth curves over the entire frequency band it was necessary to very accurately model the problem. For most of the computations we used $N=96$ in Eq. (7) and used 901 discrete points in our azimuthal integrations. The values of these parameters could be much smaller for the lower frequencies but we used the same values for the entire curve. The wave-number integrals for the Green's function kernels were carried out from $k_x=-10\omega/1500$ to $10\omega/1500$ with 3000 integration steps. These various parameters were varied in other computations of the same curves to make sure that stable results were being obtained.

The spectral curves for the object totally within the water column show the most variation as a function of frequency—as the object becomes increasingly buried these curves become increasingly smooth and eventually become similar to the free space curve. These results are reasonable—for the object above the interface, there are the effects of the scattering from the cylinder itself, but there are also multiple scattering interactions between the interface and the object. As the object is increasingly buried to the 50% level, there is less and less ''space'' between the object and the interface in which the multiple scattering interactions can take place. As the object moves into the lower half-space, more space opens up between the cylinder and the interface. However, the situation is different than when the cylinder is in the upper half-space, because now the incident energy on the cylinder (from both the incident field and from multiple interactions with the interface above) is all downgoing. In the case where the cylinder was mostly above the interface, the incident energy was both downgoing and upgoing. We can see that as the cylinder becomes totally buried, the spectral curve becomes very similar to the free space curves of Fig. 3. However, the mean levels are reduced by about 3–4 dB. With respect to cylinder burial, we also see a decrease in the mean level of the curves of Fig. 4 as the cylinder becomes increasingly buried. However, this decrease is not uniform with respect to frequency. For example, there are frequencies in Fig. 4(a) and (b) corresponding to a significant null; many of these frequencies are no longer in a null in the curves of Fig. 4(c)–(e).

We now consider a 0.5-m radius cylinder with a 5-mm-thick shell buried 25% (see Fig. 5). The shell has parameters $c=5000$ m/s and $\rho=3000$ kg/m^3 (i.e., the same parameters as the cylinder considered before) and the interior has the values $c=340$ m/s and $\rho=1.2$ kg/m^3. These values are rep-

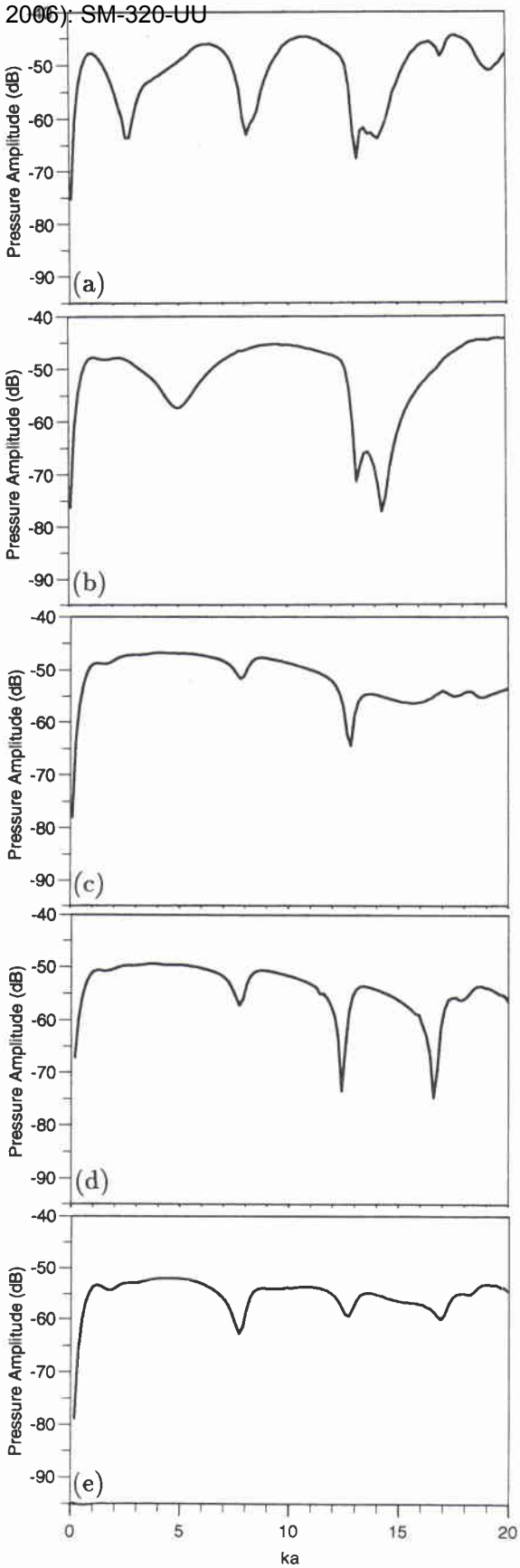

FIG. 4. Spectrum of backscattered field for 1-m-radius cylinder $c_c=5000$ m/s, $\rho_c=3000$ kg/m^3 ($x_s=-50$ m $z_s=25$ m) for cylinder center (a) 1.01 m above interface, (b) 0.5 m above interface, (c) 0.0 m above interface, (d) 0.5 m below interface (e) 1.01 m below interface.

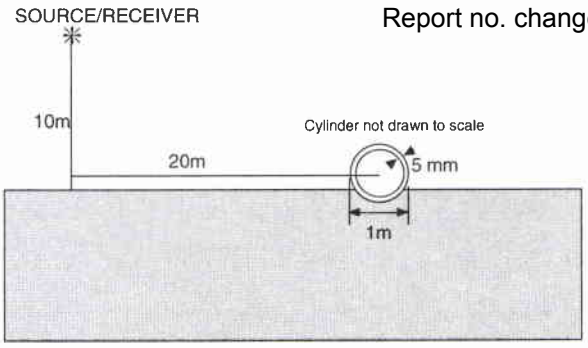

FIG. 5. Schematic diagram of the geometry used for the computation of the backscattering from a shelled cylinder.

resentative of air. Because of the slight thickness of the shell, we expect the cylinder to scatter as if a pressure release surface. In this example, the source is taken to be at $x_s = -20$ m and $z_s = 10$ m. In Fig. 6 we show the computed spectral curve for a receiver at the source point. Once again we compute to a ka product of 20; since the radius of the cylinder is now 0.5 m this corresponds to a frequency of approximately 9550 Hz. We also show in Fig. 6 with the solid curve the spectral response of the same cylinder in free space. As can be seen, this curve is basically flat and hence the structure of the cylinder's spectral curve (dashed line) is due to the interaction of the incident and scattered field with the interface. However, we have computed this curve with quite a frequency increment of 4 Hz in contrast to the 80 Hz spacing used for the BIEM curve and small, very thin resonances are visible. To see if these features were present in the BIEM spectral curve we computed a curve for 25 frequencies ($\Delta f = 1.2$ mHz) about the ka value of 12.719, which corresponds to a peak in the free-space curves of Fig. 5. As can be seen in Fig. 7 the peak is also present in the BIEM spectral curve (dashed line)—the peak location is very close to that of the free-space curve (solid line) which recomputed with the

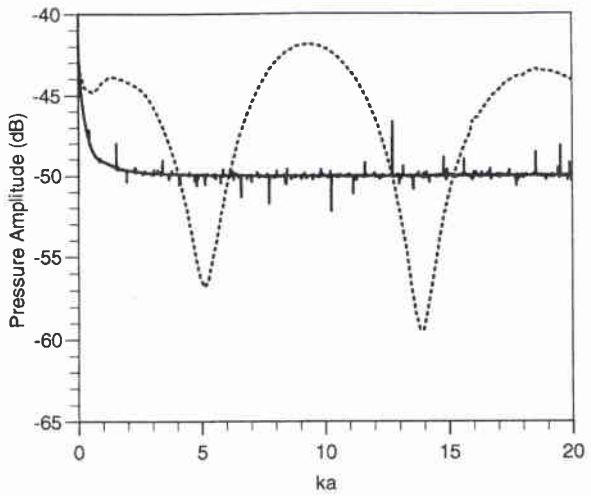

FIG. 6. Spectrum of backscattered field for 0.5-m-radius, air-filled cylinder with 5-mm-thick shell ($x_s = -20$ m $z_s = 10$ m) with cylinder center 0.25 m above interface. The solid line is the free-space curve (surrounding velocity is 1500 m/s) computed with a frequency spacing of 4 Hz. The dashed line is the BIEM curve computed with a frequency spacing of 80 Hz.

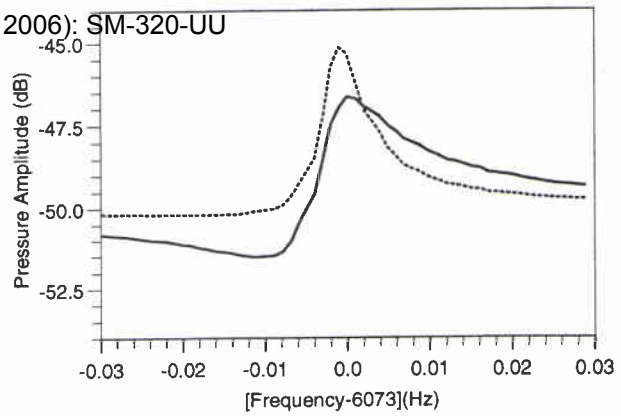

FIG. 7. High resolution spectrum of backscattered field for shelled cylinder for $ka \approx 12.719$ (frequency = 6073.0 Hz) for free-space curve (solid line) (surrounding velocity = 1500 m/s) and for cylinder (dashed line) 25% buried in sediment. A frequency spacing of $\Delta f = 1.2$ mHz was used for both curves.

same frequency increment as the fine resolution BIEM curve. The shape of these two curves is, however, somewhat different.

In Figs. 8 and 9 we show two-dimensional grayscale plots of the total pressure field for the larger homogeneous cylinder and for the smaller shelled cylinder. These fields were computed for a frequency corresponding to a ka product of 10. The frequency for the smaller cylinder case is double that of the larger cylinder computation. In both cases, a shadow zone behind the cylinder is evident. The cylinder is shaded in with the highest contour color—this is not the computed value within the cylinder. For the smaller cylinder, the cylinder surface (or just below the surface) appears as a pressure release surface and the pressure goes to zero there.

III. SUMMARY

We have presented in this paper a BIEM which combines the form of the solution for the interior acoustic field in a layered cylinder with the exterior Green's function for a two-half-space medium. The Green's function is decomposed into singular Hankel function terms with coefficients

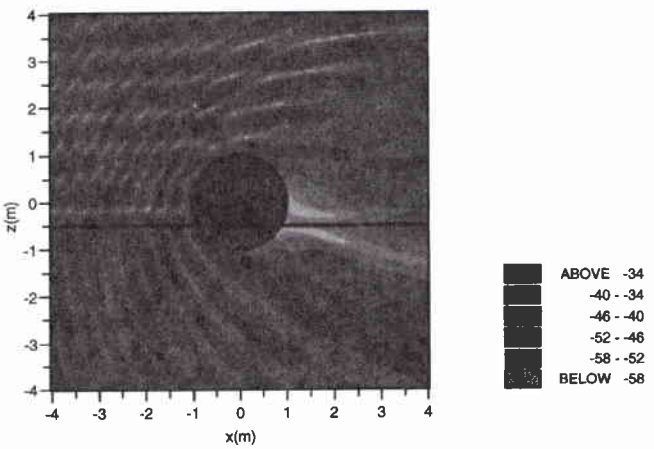

FIG. 8. Two-dimensional grayscale plot of amplitude (dB) of total pressure field for 1-m-radius cylinder (25% burial) computed for $ka = 10$.

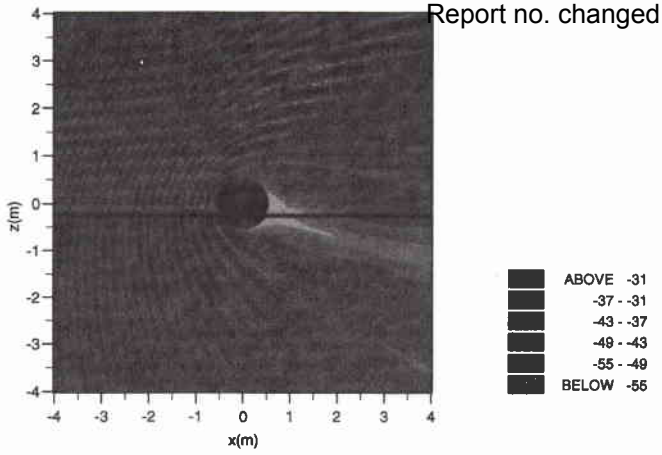

FIG. 9. Two-dimensional gray scale plot of amplitude (dB) of total pressure field for 0.5-m-radius cylinder (25% burial) computed for $ka = 10$.

dependent upon the density contrast of the medium and wave-number integrals. The BIEM was used to compute the spectral curves, for a particular backscatter geometry, as the scattering cylinder became increasingly buried in the lower half-space. The spectral curves for the cylinder in the upper half-space were significantly different in appearance than the free-space curves; as the cylinder became increasingly buried, the spectral curves became smoother and appeared more like the free-space result (although reduced in amplitude). We also used the method to computed the scattered field from a shelled cylinder. Two-dimensional plots of the pressure field in the neighborhood of partially buried cylinders (solid and shelled) were computed.

It should be possible to extend the approach of this paper to consider three-dimensional scattering from spheres; in particular, by using azimuthal symmetry it should be possible to solve a sequence of two-dimensional problems, one for each azimuthal order. In the future, we would also like to consider elastic scattering problems for a partially buried object.

[1] P. Gerstoft, and H. Schmidt, "A boundary element approach to seismo-acoustic facet reverberation," J. Acoust. Soc. Am. **89**, 1629–1642 (1991).
[2] R. Lim, J. Lopes, R. Hackman, and D. Todoroff, "Scattering by objects buried in underwater sediments: Theory and experiment," J. Acoust. Soc. Am. **93**, 1762–1783 (1993).
[3] A. Sarkissian, "Multiple scattering effects when scattering from a target in a bounded medium," J. Acoust. Soc. Am. **96**, 3137–3144 (1994).
[4] R. Lim, "Acoustic scattering by a partially buried three-dimensional elastic object," J. Acoust. Soc. Am. **99**, 2498 (1996).
[5] P. K. Banerjee, *The Boundary Element Methods in Engineering* (McGraw-Hill, Maidenhead, England, 1994).
[6] H. A. Schenck, "Improved integral formulation for acoustic radiation problems," J. Acoust. Soc. Am. **44**, 41–58 (1968).
[7] F. B. Jensen, W. A. Kuperman, M. B. Porter, and H. Schmidt, *Computational Ocean Acoustics* (AIP, New York, 1994).
[8] J. A. Fawcett, "The Computation of the Scattered Pressure Field From A Cylinder Embedded Between Two Half-Spaces With Different Densities," J. Acoust. Soc. Am. **99**, 2435–2438 (1996).
[9] M. Abramowitz and I. Stegun, Eds., *Handbook of Mathematical Functions* (Dover, New York, 1970), Chap. 9.
[10] J. Stratton, *Electromagnetic Theory* (McGraw-Hill, New York, 1941).
[11] T. W. Dawson and J. A. Fawcett, "A boundary integral method for acoustic scattering in a waveguide with non-planar surfaces," J. Acoust. Soc. Am. **87**, 1110–1125 (1990).

The computation of the scattered pressure field from a cylinder embedded between two half-spaces with different densities

John A. Fawcett
SACLANT Undersea Research Centre, Viale San Bartolomeo 400, 19138 San Bartolomeo (SP), Italy

(Received 11 August 1995; accepted for publication 6 December 1995)

In this Letter a straightforward, efficient method for computing the acoustic field scattered by a cylinder embedded halfway between two half-spaces is presented. These half-spaces have the same velocity but a different density. This method should be useful for benchmarking more general codes.

PACS numbers: 43.30.Gv, 43.20.Fn

INTRODUCTION

There have been a variety of methods proposed for the solution of waveguide scattering problems (for example, Refs. 1–3). The last two references, however, are not applicable in the case that the scattering object is embedded in an interface between two media. In this letter, we give a semi-analytical solution to the problem of a cylinder embedded between two half-spaces with only a discontinuity in density (although, the sound speed can be different within the cylinder). Although this is certainly a very particular subset of the general scattering problem, we feel that our method of solution could provide useful benchmarks for more general numerical codes.

I. THEORY

Consider a half-space with the upper medium having sound speed c_1 and density ρ_1 and the lower medium, sound speed $c_2=c_1$ and density ρ_2. A cylinder with sound speed c_c, density ρ_c, and radius a is embedded halfway between the two medium (see Fig. 1). The theory described below also applies to a cylinder with internal cylindrical layering but we will only consider a homogeneous cylinder here.

A. Form of solution within half-space

We consider a polar coordinate system based at the center of the cylinder. The Helmholtz equation in this system is

$$\frac{1}{r}\frac{\partial}{\partial r}\left(r\frac{\partial p}{\partial r}\right)+\frac{1}{r^2}\frac{\partial^2 p}{\partial \theta^2}+\frac{\omega^2}{c^2}p=0 \quad \left[\frac{\delta(r-r_s)\,\delta(\theta-\theta_s)}{r_s}\right], \tag{1}$$

where we have indicated on the right of Eq. (1) the form of a possible point source. We seek a solution of Eq. (1) in the form

$$p(r,\theta)=\sum_{n=0}^{\infty}\Theta_n(\theta)R_n(r). \tag{2}$$

The eigenvalue problem

$$\frac{d^2\Theta_n}{d\theta^2}=\lambda_n\Theta,$$

$$\Theta_n(\theta=0^+,\pi^+)=\Theta_n(\theta=0^-,\pi^-), \tag{3}$$

$$\frac{1}{\rho_1}\frac{\partial\Theta_n}{\partial\theta}(\theta=0^+,\pi^+)=\frac{1}{\rho_2}\frac{\partial\Theta_n}{\partial\theta}(\theta=0^-,\pi^-),$$

can be easily solved in terms of sine and cosine functions. There are two sets of eigenfunctions

$$\phi_n(\theta)=\frac{1}{C_n}\cos(n\theta), \quad 0\leqslant\theta\leqslant 2\pi \tag{4a}$$

and

$$\psi_n(\theta)=\frac{1}{S_n}\sin(n\theta), \quad 0\leqslant\theta\leqslant\pi;$$

$$=\frac{1}{S_n}\frac{\rho_2}{\rho_1}\sin(n\theta), \quad \pi\leqslant\theta\leqslant 2\pi. \tag{4b}$$

In Eq. (4) C_n and S_n are the normalizations of the modes and are equal to

$$\left(\int_0^{2\pi}\frac{\phi_n^2}{\rho(\theta)}\,d\theta\right)^{1/2}, \quad \left(\int_0^{2\pi}\frac{\psi_n^2}{\rho(\theta)}\,d\theta\right)^{1/2},$$

respectively. A similar type of eigenfunction expansion was previously used by Chu[4] for an exact solution of propagation in a density contrast wedge.

Multiplying Eq. (1) by ϕ_n (or also by ψ_n) and dividing by $\rho(\theta)$ and integrating from 0 to 2π we obtain the radial equation for the modal coefficients,

$$\frac{1}{r}\frac{\partial}{\partial r}\left(r\frac{\partial R_n}{\partial r}\right)-\frac{n^2}{r^2}R_n+\frac{\omega^2}{c^2}R_n=0 \quad \left[\frac{\delta(r-r_s)\,\phi_n(\theta_s)[\psi_n]}{\rho(\theta_s)}\right]. \tag{5}$$

Equation (5) has a standard solution in terms of Hankel and Bessel functions. Thus the pressure field has the general form

 0001-4966/96/99(4)/2435/4/$6.00

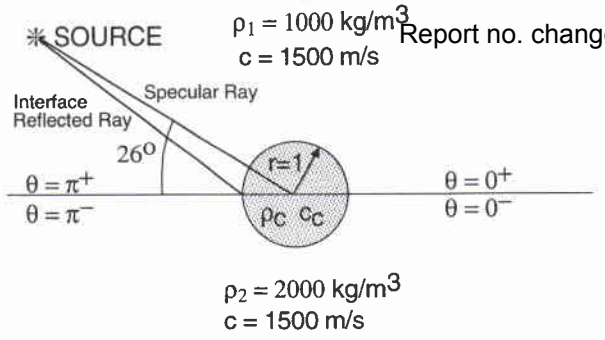

FIG. 1. Schematic diagram of cylinder embedded between two half-spaces.

$$p(r,\theta)=\sum_{n=0}^{\infty}\phi_n(\theta)(\gamma_n J_n(kr)+a_n H_n^{(1)}(kr))$$

$$+\sum_{n=1}^{\infty}\psi_n(\theta)(\tau_n J_n(kr)+b_n H_n^{(1)}(kr)), \qquad (6)$$

where $k\equiv\omega/c_1$. For the scattering solution from a cylinder the γ_n,τ_n are known incident coefficients and a_n,b_n are to be determined. The incident coefficients are determined from Eq. (5) with the radial source,

$$\gamma_n=(-i\pi/2)\phi_n(\theta_s)H_n(kr_s)/\rho(\theta_s) \qquad (7a)$$

and

$$\tau_n=(-i\pi/2)\psi_n(\theta_s)H_n(kr_s)/\rho(\theta_s). \qquad (7b)$$

B. Form of the solution for a cylindrical inclusion

In order to determine a_n,b_n we invoke the boundary conditions at the surface of the cylinder,

$$p(r=a,\theta)=p^{\mathrm{cyl}}(r=a,\theta) \qquad (8a)$$

and

$$\frac{1}{\rho(\theta)}\frac{\partial p}{\partial r}(r=a,\theta)=\frac{1}{\rho_c}\frac{\partial p^{\mathrm{cyl}}}{\partial r}(r=a,\theta). \qquad (8b)$$

The solution within the cylinder is expressed in the form

$$p^{\mathrm{cyl}}(r,\theta)=\sum_{n=0}^{\infty}c_n J_n(k_c r)\cos(n\theta)$$

$$+\sum_{n=1}^{\infty}d_n J_n(k_c r)\sin(n\theta). \qquad (9)$$

We multiply Eq. (8a) by $\phi_n(\theta)/\rho(\theta)$ or $\psi_n(\theta)/\rho(\theta)$ and integrate from 0 to 2π; similarly we multiply Eq. (8b) by ϕ_n or ψ_n and integrate from 0 to 2π. This procedure gives a set of equations for a_n, b_n, c_n, and d_n in terms of the known incident coefficients. For the formulation outlined above the submatrices of the larger coefficient matrix corresponding to the coefficients a_n and b_n are diagonal; the remainder of the coefficient matrix involves coupling terms of the form

$$\int_0^{2\pi}\frac{1}{\rho(\theta)}\psi_i(\theta)\cos(j\theta)d\theta, \quad \int_0^{2\pi}\frac{1}{\rho(\theta)}\phi_i(\theta)\cos(j\theta)d\theta$$

and

$$\int_0^{2\pi}\frac{1}{\rho_c}\psi_i(\theta)\cos(j\theta)d\theta, \quad \int_0^{2\pi}\frac{1}{\rho_c}\phi_i(\theta)\cos(j\theta)d\theta.$$

There are also the analogous integrals involving the $\sin(j\theta)$ terms. These integrals are divided into the intervals $[-\pi,0]$ and $[0,\pi]$ and evaluated analytically. In the formulation of this paper we define our unknown coefficients to include the Hankel/Bessel function evaluated at $r=a$. This is done in order to avoid excessively large or small values for the coefficients corresponding to large angular orders. The infinite series of Eqs. (6) and (9) are truncated at finite N and the system of equations is then solved for the unknown coefficients. With these coefficients the solution can be generated at any point.

II. NUMERICAL EXAMPLE

We first consider a rigid cylinder of radius $a=1$ m. Our program does not explicitly implement rigid boundary conditions but we simulate these by setting $c_c=50000$ m/s and $\rho_c=10^7$ kg/m^3. The upper embedding medium has sound speed $c_0=1500$ m/s and $\rho_1=1000$ kg/m^3; the lower medium has sound speed $c_0=1500$ m/s and $\rho_2=2000$ kg/m^3. The line source is located at $x=-200$ m and $z=100$ m and we consider a receiver at the same point. The source is at an angle of 26° with respect to the center of the cylinder. In terms of ray theory there is a ray which specularly reflects off the cylinder; there is also a ray which reflects off the medium interface, reflects off the cylinder and returns to the receiver, and the same ray first reflects off the cylinder, reflects off the interface and then returns to the receiver. However, for the geometry of the cylinder half-buried this ray is degenerate; it reflects off the cylinder at the cylinder–interface intersection (see Fig. 1). The two reflected rays (the specular and the interface/cylinder) for this problem interfere constructively and destructively with each other; by calculating the difference in their path lengths (two-way) it is possible to deduce that as frequency is varied, the peak-to-trough amplitude variation of this interference corresponds to $\Delta ka=\Delta\omega/c\approx 15.5$. In all our computations we used $N=100$ in the sums of Eqs. (6) and (9). In Fig. 2 we plot the amplitude of the backscattered field (dashed line) [multiplied by $\sqrt{ka}$ to compensate for the variation of the energy from the incident field $iH_0^1(kr)/4$] as a function of $ka=\omega/1500$. We also show the analogous curve (solid line) for the case of $\rho_2=1000$ kg/m^3. This corresponds to the cylinder in free space. The free-space curve is oscillatory for small values of ka but levels off asymptotically for larger values; the density contrast case is similar but exhibits the amplitude modulation as described above.

We now consider a penetrable cylinder. The acoustic parameters are $\rho_c=1500$ kg/m^3 and $c_c=1700$ m/s. In Fig. 3 we show the curves for the density contrast background medium (dashed line) and for free space (solid line). In this example, the two curves have a periodic character. This is due to the fact that there is now reverberation of energy within the cylinder (in contrast to the previous rigid case). The two-way distance across the cylinder is 4 m. Over this distance the required change in ka for a phase change of 2π is $\Delta ka=1.78$ which is consistent with the periodic spacing

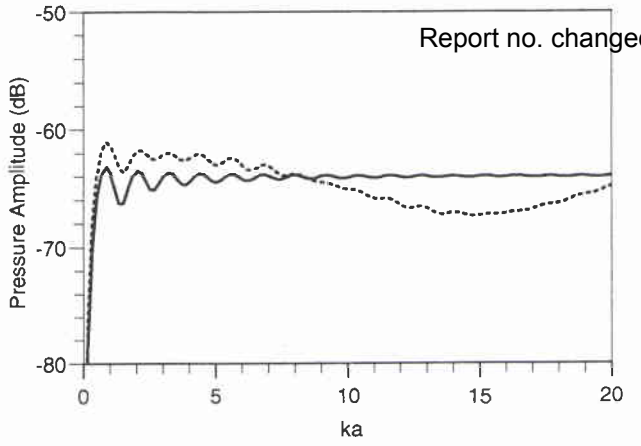

FIG. 2. Spectrum of backscattered field for "rigid" cylinder embedded between two half-spaces with density contrast (dashed) and no density contrast (i.e., free space) (solid).

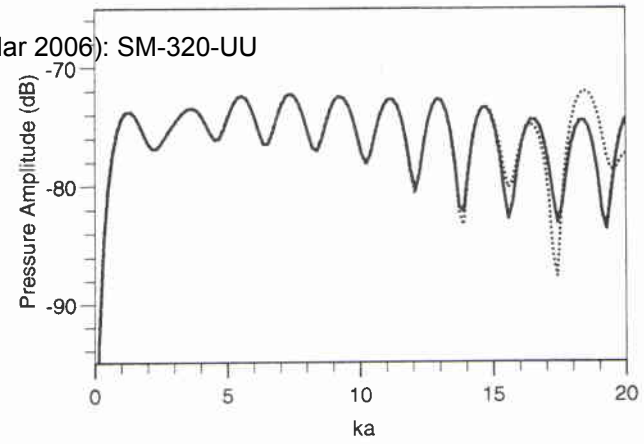

FIG. 4. Spectrum of backscattered field for penetrable ($\rho_c = 1500$ kg/m^3, $c_c = 1700$ m/s) cylinder embedded between two half-spaces with density contrast using 15 terms (dotted), 50 terms (dashed), and 100 terms (solid) in the Fourier/Modal expansion series.

seen in Fig. 3. However, as can be seen, there are significant differences in detail between the two curves. In particular, for the higher ka values the spectrum for the embedded cylinder has its peaks in the nulls of the free-space cylinder. It is not surprising that the curves are so different; the plane-wave reflection coefficient along the lower interior surface of the cylinder is quite different when the ratio of densities is 1.5:2 (density contrast case) rather than 1.5:1 (free space case). For example, the normal incidence reflection coefficient along the lower interior surface of the cylinder is positive in the former case rather than negative as in the case of the free-space cylinder.

In order to test the convergence of the Fourier–Modal expansion, we computed the solutions of the two above examples for $N=50$ and $N=100$ in the series of Eq. (9); there was virtually no difference in the results. In Fig. 4 we show the resulting curves for the penetrable cylinder with the density-contrast basement for $N=15$ (dotted), $N=50$ (dashed), and $N=100$ (solid) terms. As can be seen, the $N=100$ and $N=50$ curves are essentially indistinguishable.

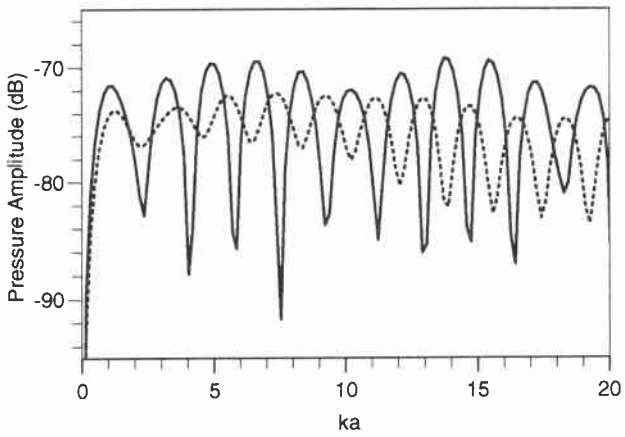

FIG. 3. Spectrum of backscattered field for penetrable ($\rho_c = 1500$ kg/m^3, $c_c = 1700$ m/s) cylinder embedded between two half-spaces with density contrast (dashed) and no density contrast (i.e., free space) (solid).

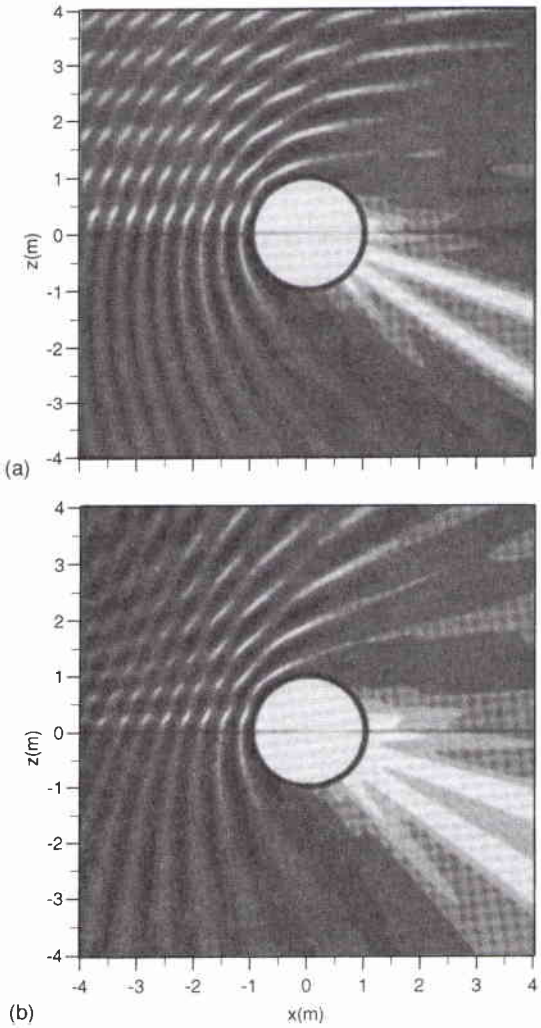

FIG. 5. Two-dimensional pressure amplitudes for rigid cylinder with density-contrast basement ($ka=10$) for source located at (a) $x_s = -200$ m, $y_s = 100$ m (grayscale levels with increment -3 dB from below -55 dB to above -43 dB) (b) $x_s = -6$ m, $y_s = 3$ m (grayscale levels with increment -3 dB from below -40 dB to above -28 dB).

The $N=15$ curve is in agreement with the other two curves until approximately $ka=15$. In general, for transmission and of ka a larger number of terms in the series is required. The same type of behavior is also true for the rigid cylinder case.

Finally, we present full field computations in Fig. 5(a) and (b) for a source at $x=-200$ m, $y=100$ m and $x=-6$ m, $y=3$ m, respectively. The fields are not computed within the cylinder. The grayscale levels are different for the two plots (from below -55 dB to above -43 dB, and from below -40 dB to above -28 dB, respectively) but the amount of dB variation for the two is the same. These fields are computed for a frequency of $15\,000/(2\pi)$ Hz which corresponds to $ka=10$ and are shown for a 8-m square about the cylinder. The cylinder and half-space parameters are those of the rigid cylinder, density-contrast example. In both cases the shadow zone behind the cylinder is evident; it can be seen that there is some structure in this zone. The shadow zone appears to be wider in the case of the closer source [Fig. 5(b)]. On the source side of the cylinder the interference pattern between the incident and backscattered fields can be seen in the two figures.

III. SUMMARY

We have given a simple, efficient method for computing the field scattered by a cylinder embedded in a medium with a density jump. The cylinder was taken to be halfway between the two half-spaces. It is probably possible to relax this restriction of 50% burial by considering the modes of the outer medium to be referred to a different origin (i.e., displaced vertically) than that of the cylinder. One could still use modal projection in this case to derive a system of equations for unknown coefficients. However, the theory and implementation are not as straightforward for this more general case.

[1] P. Gerstoft and H. Schmidt, "A boundary element approach to seismo-acoustic facet reverberation," J. Acoust. Soc. Am. **89**, 1629–1642 (1991).
[2] R. Lim, "Scattering by an obstacle in a plane-stratified poroelastic medium: Application to an obstacle in ocean sediments," J. Acoust. Soc. Am. **95**, 1223–1244 (1994).
[3] J. Fawcett, "A plane-wave decomposition method for modeling scattering from objects and bathymetry in a waveguide," submitted to J. Acoust. Soc. Am. 1995.
[4] D. Chu, "Exact solution for a density contrast shallow water wedge using normal coordinates," J. Acoust. Soc. Am. **87**, 2442–2450 (1990).

Report no. changed (Mar 2006): SM-320-UU

Document Data Sheet

NATO UNCLASSIFIED

Security Classification		Project No.
NATO UNCLASSIFIED		033-3
Document Serial No.	**Date of Issue**	**Total Pages**
SM-320	December 1996	18 pp.

Author(s)

Fawcett, J. A.

Title

Modelling scattering from partially buried cylinders

Abstract

1. A boundary integral equation method is presented for the computation of the acoustic field scattered from a cylindrical object which is totally within the water column, totally buried in sediment, or partially buried. The unknown field quantities within the cylindrical object (which may have internal cylindrical layering) are represented by a Fourier/Bessel series with unknown coefficients. The pressure field and its radial derivative on the exterior of the cylinder are related to this series and a system of equations for the unknown coefficients derived. This method is used to compute the spectral curves for the backscattered field as a function of cylinder burial. Some two-dimensional full-field computations for scattering from cylindrical objects are also presented.

2. Various methods have been proposed for the solution of waveguide scattering problems (1-3). The last two references however are not applicable in the case of a scattering object embedded in an interface between two media. A semi-analytical solution is given to the problem of a cylinder embedded between two half-spaces with only a discontinuity in density (although the sound speed can be different within the cylinder). Although this is a particular subset of the general scattering problem, this method could provide useful benchmarks for more general numerical codes.

Keywords

Sea surface scattering

Bottom scattering

Mine detection

Issuing Organization

North Atlantic Treaty Organization
SACLANT Undersea Research Centre
Viale San Bartolomeo 400, 19138 La Spezia, Italy

[From N. America: SACLANTCEN CMR-426 (New York) APO AE 09613]

Tel: +39 (0)187 540 111
Fax:+39 (0)187 524 600

E-mail: library@saclantc.nato.int

NATO UNCLASSIFIED

Initial Distribution for SM-320

SCNR for SACLANTCEN		*National Liaison Officers*	
SCNR Belgium	1	NLO Canada	1
SCNR Canada	1	NLO Denmark	1
SCNR Denmark	1	NLO Germany	1
SCNR Germany	1	NLO Italy	2
SCNR Greece	2	NLO Netherlands	1
SCNR Italy	1	NLO UK	3
SCNR Netherlands	1	NLO US	4
SCNR Norway	1		
SCNR Portugal	1		
SCNR Spain	1		
SCNR Turkey	1		
SCNR UK	1		
SCNR US	2		
French Delegate	1		
SECGEN Rep. SCNR	1	Total external distribution	34
NAMILCOM Rep. SCNR	1	SACLANTCEN Library	26
SACLANT	3	Total number of copies	60